Comparison of features from SAR and GMTI imagery of ground targets

David Beckman* and Samuel Frame

Toyon Research Corporation, 75 Aero Camino Drive Suite A, Goleta, CA USA 93117-3139

ABSTRACT

We describe an algorithm for class-independent automated target recognition (ATR) and association using range-Doppler images of moving targets and SAR images of stationary targets. This algorithm can be used both for target identification (by comparison against a pre-existing database of measurements of all potential targets) and target association (not requiring a pre-existing database). The algorithm computes a one-dimensional signature for each received range-Doppler image; these signatures are stored in a database for comparison against other detections. The signatures used in our algorithm are range profiles, generated from the clutter-suppressed, filtered image by incoherently integrating the image energy across a number of Doppler bins centered on the target. The result is then normalized, to remove information about the overall cross-section from the profile, and range-aligned with other collected profiles by matching the profile centroids. Statistical models of the profiles are created as the targets are tracked, and newly-created profiles are compared against the existing models by computing the likelihood of the new profile given a particular model.

Keywords: features, signatures, association, identification

1. BACKGROUND

A common problem arising in kinematic tracking of multiple targets in a region is of *misassociation* between existing tracks and new detections. This can occur, for example, when the distance between two targets becomes small enough that detections from either target can easily be mistakenly assigned to the other, or when a target makes a state transition (such as a move-stop transition) unpredicted by its tracker. After such a misassociation, further kinematic measurements are very unlikely to resolve the identity ambiguity between these two targets.

One way to solve this problem, at least in principle, is to increase the frequency and the accuracy of the kinematic measurements until such ambiguities no longer arise. This is unfortunately difficult to do in practice. Such high revisit rates require large numbers of sensors even under optimum conditions; uneven terrain makes the requirements even more unrealistic.

A much more forgiving technique is the use of extra information typically present in sensor measurements. The sensor return from a target may contain information beyond mere kinematic information such as position and velocity; the radar cross-section of a vehicle is a simple example of such extra information. Generally we will call such extra information a *feature* or *signature* of a measurement. If different vehicles have different signatures, then the vehicles may be distinguished at any time by measurement of this signature.

There are two different methods for using such information. First, the measurement feature may be matched against a previously constructed database of measurement features to try to determine the actual identity of each target being tracked, a "class-dependent" approach. One advantage of this scheme is that it provides an absolute identification for a vehicle. Another is that the measurements used to create the database may be made at any time; the database can be constructed well before it is actually needed, when resource management is not a major issue. A disadvantage of this scheme is that use of an incomplete database, in which not all targets in the scenario have entries, will result in identification errors or unidentifiable targets.

The other method for using measurement features is to directly compare different measurement features made during the scenario, a "class-independent" approach. Of course, this method has just the opposite advantages and disadvantages of the class-dependent approach: It does not require that the vehicles in the scenario be of

*dbeckman@toyon.com; phone (805)968-6787x133; fax (805)685-8089; www.toyon.com

previously-encountered types; but it does not provide absolute identification, and, since resource limits will make it difficult in general to fully characterize the features for a particular vehicle track, noise and clutter sources have the potential to degrade the fidelity of the comparison more than with the first, class-dependent, approach.

An important component of each of these methods, and the emphasis of this paper, is a *feature association algorithm*, an algorithm for determining whether two different sets of measurement features are likely to have come from the same target. The demands of such an algorithm made by these two methods are slightly different: For the first approach, we expect there to be more measurements in the database than made during the scenario, while in the second approach we expect the two sets to be roughly equal in size. To be useful for both approaches, a feature association algorithm should be able to handle feature sets of different sizes and with different noise and clutter densities.

There are many different types of features, with many different properties and different uses. Each different type of sensor will have its own set of measurable target features. Ideally, the algorithm would be able to associate measurements made by different types of sensors, aiding the sensor fusion problem as well as the tracking problem. In the class-dependent approach, this is not difficult: the feature database may contain information about a wide variety of features, allowing identification of a target from several different sensors.

In the class-independent approach, however, this is a more interesting problem. Different features—for example, features from two different sensors—will not in general be comparable without further knowledge of the possible targets. In some cases, however, we expect (due, for example, to knowledge about the behavior of the particular features and the physics of the sensors) that similar features will be comparable across sensors. The ideal feature would be persistent across different sensor measurement modes, making association and sensor fusion relatively straightforward (as well as reducing the necessary size of the database, for the feature-dependent approach).

2. HIGH-RESOLUTION RANGE MEASUREMENTS

The feature association algorithm described in this paper is based on the use of *high-resolution range-profile* (HRR) features in radar measurements. A range profile measures some property of the radar return from a target as a function of increasing range across the target. Although the cross-range resolution of an imaging radar mode depends on the coherent integration time for that mode, the range resolution is governed primarily by the radar transmitter and receiver bandwidth; so it may be relatively constant over radar modes. This is one motivation for considering a range-parametrized feature. In addition, for many radar imaging modes we can consider a suitable integration over the cross-range direction as computing the total radar energy returned as a function of range, a value that should be mostly independent of parameters other than the sensor wavelength and the target aspect (along with environmental parameters such as noise and clutter density). Below we will discuss some of the details of profile creation for different types of sensor data.

The aspect dependence of HRR features makes the association problem more complicated. HRR features measured at substantially different aspects, even of the same target, should not be expected to be similar. Thus for a class-dependent association algorithm, the feature database must contain information about the features not just for all expected targets, but for all expected targets *at all expected aspect angles*.* For a class-independent algorithm, feature-aided association as a target moves through a close encounter with a second target may be difficult if the target aspect changes through the encounter—for example, if the target turns. A more sophisticated tracker may be required to deal adequately with such cases: for example, by making feature associations between vehicles before and after the encounter, and extrapolating the after-encounter track back in time to the encounter to complete the track.

This decorrelation angle may be estimated given the range resolution δr of the radar. Consider the case of two scatterers at the same range but at opposite sides of the object, a distance d apart. When the object's aspect changes by a small angle $\delta\phi$, the range of one scatterer changes by about $d\,\delta\phi$ relative to the other. We should expect significant decorrelation between two profiles by the time they are separated in angle by enough

*The aspect angle must include at least azimuth and elevation angles. For articulated targets, in general more variables are needed to describe the target's internal state. We will use the word "aspect" to describe all such necessary internal state variables, as well as those describing the target's orientation.

that these two scatterers migrate to different range bins: $d\,\delta\phi \geq \delta r$, i.e. when $\delta\phi \approx \frac{\delta r}{d}$. For SAR images having resolution sufficient for target identification, and targets a few meters in diameter, this decorrelation angle is typically a few degrees. The feature association algorithm needs to fuse kinematic information, from both the measurement and the potentially-matching tracks, to determine the possible aspects for the feature. We will describe this fusion procedure below.

But this extra complication can be a blessing as well as a curse. The aspect dependence of these features means that there is aspect information encoded in the feature along with the identification information. Thus HRR features can be used to measure the target aspect angle, with accuracy $\sim \delta\phi$, and hence to gain additional kinematic information about the target which is not available in a purely kinematic $(r, \phi, \dot{r})$ measurement.

3. HRR PROFILE CREATION ALGORITHM

The basic idea behind computation of an HRR feature given a radar image, as stated above, is simple: just integrate the target energy in the image over its non-range directions. Different image types present different subtleties, however; in practice we must carefully consider how to perform this integration in each case. Broadly, we divide the profile creation process into three stages: an image preprocessing stage, the creation of the actual profile, and a profile postprocessing stage. We will consider these three stages in detail for the cases of SAR and MTI range-Doppler images.

First, in order to provide a motivation for the later discussion, we detail the core of the profiling algorithm: the creation of an HRR profile $\mathbf{y}$ from a multidimensional radar image. As already mentioned, this is just a sum of the pixel energies over the cross-range directions:

$$y_r = \sum_{x=x_{\min}}^{x_{\max}} E_{rx} = \sum_{x=x_{\min}}^{x_{\max}} |V_{rx}|^2 \,, \tag{1}$$

where we use r and x to represent the range and cross-range coordinates, V_{rx} is the complex voltage image, and $E_{rx} = |V_{rx}|^2$ is the energy (intensity) image. The summation range is chosen to include as many pixels containing significant target return, and as few pixels containing significant clutter return, as practical. This summation range depends on the image properties, and choosing it is an important aspect of the image preprocessing stage.

This cross-range integration is actually just the simplest in a large class of profiling algorithms. More generally we may consider integrating the nth cross-range moment of the image with a nonconstant kernel $k(x)$:

$$y_r^{(n,k)} = \Big[\sum_{x=x_{\min}}^{x_{\max}} k(x)\, |V_{rx}|^n \Big]^{2/n} \,; \tag{2}$$

with this terminology the above profiling algorithm is $y_r \equiv y_r^{(1,1)}$. Another interesting profiling algorithm in this class is the *dominant-scatterer* algorithm $y_r^{(\infty,1)}$ suggested by Hodges,[1] in which a range-profile element has the maximum energy over all image elements at that range.

3.1. SAR images

A SAR image is formed by recording the coherent radar returns from the target region as the sensor moves along a trajectory. The phase-history data is then processed to generate an image by inverting the impulse response.[2] For a sensor flying a nearly-straight trajectory and imaging a distant target, this inversion can be computed with an FFT, making it computationally tractable even for fairly large images. The resulting image gives a two-dimensional map of radar return intensities over the target region, including returns from both target and clutter.

The target return is typically well localized in a well-focused SAR image (though if the target contains strong reflectors, multipath effects may create target "echoes" at greater ranges than the primary target return). So an obvious candidate for image preprocessing is segmentation: Once the target is detected in the image, we should be able to mask out most of the clutter in the image (possibly retaining some clutter behind the image to capture

any multipath returns). In our tests, the target-to-clutter ratio was sufficiently high that this segmentation could be done easily, and the cross-range integration can be done essentially over just the target pixels.

The cross-range resolution for a SAR image is limited by the angle range over which the coherent integration is done. For high-resolution SAR images useful for identification of stationary targets this angle range is typically a few degrees. However, as outlined above, HRR profiles can be expected to decorrelate over an angle range $\delta\phi \sim 1°$; this means that a single SAR image contains information from several possibly-distinguishable HRR profiles. In order that the created profiles are comparable with profiles created from images having a smaller angle span, we must divide each SAR image into subimages with lower resolution, each one equivalent to a SAR image created over a smaller angle range.

To do this, the SAR image's azimuth processing is inverted (after the clutter masking) to give a *range-angle map* (the "angle" coordinate is the sensor-target aspect angle, changing as the sensor platform flies its course) spanning a few degrees in azimuth. This map is subdivided into submaps spanning about 1° in azimuth, small enough that we expect the HRR target profile to be nearly constant over the submap. From each such map we will generate a SAR image with low cross-range resolution, and from each low-resolution SAR image we will generate a single HRR profile by taking the sum (1) over the image.

One way to create a low-resolution SAR image from a range-angle submap is to simply redo the SAR processing for this smaller map. Another approach, suggested by B. Hodges of Alphatech,[1] is to subdivide (again in angle) the submap into a number of even smaller sub-submaps, process each of these as a SAR image, and incoherently average the resulting images into a single (real) SAR image. This technique may reduce variability in the image and hence in the HRR profiles.

3.2. MTI range-Doppler images

A range-Doppler image, though superficially similar to a SAR image, uses a much shorter coherent integration time, with correspondingly lower target-to-clutter levels and worse cross-range resolution. This makes stationary targets difficult to pick out of the clutter without more sophisticated processing. *Moving* targets, however, may be detected in range-Doppler images through the use of clutter cancellation, a basic form of STAP in which two antennas, one displaced along the aircraft's path relative to the other, simultaneously record the same scene, at slightly different times. Stationary objects, including most clutter, should then contribute identically to the two images, while the returns from moving objects will differ in phase.[†] Moving targets can thus be detected as a difference between the range-Doppler images created by the two antennas.

Most ground targets do not move as a unit but involve multiple differentially-moving pieces, such as treads, tires and fans. Because of this, moving ground targets often extend through many Doppler bins in a range-Doppler image. In contrast with the SAR image, the target-to-clutter ratio is typically not very large and the target "shape" in the image is not a simple function of its true spatial shape (it depends on the target's speed, as well as on what differentially-moving components are visible to the radar at the current aspect), so precisely segmenting the target pixels as in the SAR image case is not trivial. A simple solution is to segment, for example, a rectangular area out of the range-Doppler image, centered on the detected target and having sufficient size in range and Doppler to encompass the maximum expected target extent. As before, once the image is segmented we use (1) to create a HRR profile from the image.

3.2.1. SVD reduced-rank methods

Although the shape of the target in the range-Doppler image is not precisely known, if the clutter suppression is successful we expect the target to be a relatively small, relatively bright region of the image. In such a situation we may try to further filter the image using this knowledge. One set of techniques for reducing the intensity of clutter, assumed dim but occurring throughout the image, relative to that of a small bright target is the class of *rank-reduction methods*. The idea is that in the absence of clutter, the image (the target) would have low rank; for a sufficiently bright target we can use results of matrix analysis to approximate the components of the image matrix, reducing the clutter density.

[†]This assumes that the objects are not moving quickly enough to migrate substantially to other range cells, an assumption that usually holds for slowly-moving ground targets being tracked by an airborne radar.

One way to do this is based on the *singular-value decomposition* (SVD) of a matrix. The SVD of an $m \times n$ complex matrix M is the factorization

$$M = USV^\dagger \equiv \sum_k s_k \mathbf{u}_k \mathbf{v}_k^\dagger \tag{3}$$

where $U \equiv \left[\mathbf{u}_1, \ldots, \mathbf{u}_m\right] \in \mathsf{U}(m)$ and $V \equiv \left[\mathbf{v}_1, \ldots, \mathbf{v}_m\right] \in \mathsf{U}(n)$ are unitary matrices and S is a real diagonal $m \times n$ matrix. The diagonal elements s_k, ordered so that $s_1 \geq s_2 \geq \cdots$, are the *singular values* of M, and the vectors $\mathbf{u}_k$, $\mathbf{v}_k$ are the *singular vectors*.[‡] One of the important advantages of the SVD is that it is *shift-invariant*: Cyclic permutations of rows or columns of the image matrix M do not affect the singular values, and cause only cyclic shifts in the singular vectors. Thus a target need not be perfectly centered in the image in order for SVD processing to work.

For an image containing a small (and hence low-rank), bright target against a (nearly full-rank) background of clutter, the largest singular values and singular vectors typically have values close to their zero-clutter values; these singular values and vectors primarily encode information about the target. In a rank-d SVD rank-reduction method, we reconstruct the image using only the largest d singular values and vectors:

$$\tilde{M} \equiv U_d S_d V_d^\dagger \equiv \sum_{k=1}^{d} s_k \mathbf{u}_k \mathbf{v}_k^\dagger \tag{4}$$

Figure 1 demonstrates the utility and limitations of this SVD-filtering method. The SVD-reconstructed image recreates the target pixels with high fidelity, and reduces the clutter density across the image. The clutter density is not reduced uniformly across the image, however; at the same row or column as the target, the clutter density is essentially unchanged, while elsewhere in the image the target-to-clutter ratio is approximately the square of its original value. Since useful identification information in an HRR profile is only present at target ranges, we expect that integrating this SVD-filtered image over cross-range will produce an HRR profile with at best a slightly-improved target-to-clutter ratio, and hence only a slight improvement in identifiability. In tests on existing data sets, use of this this rank-reduction method moderately improved performance in some cases.

A potential solution to this problem is to perform the SVD reconstruction not on the original matrix but on a rotated version, in which the elements of M are placed on a "checkerboard lattice" in a larger matrix (with the remaining elements set to zero). As Figure 2 shows, the clutter stripes are now rotated to ranges different from the target range, and the clutter density at the target ranges is lower than before. The average clutter density over the reconstructed image, though, is larger than for the simple SVD reconstruction. In tests, this method's performance was not markedly different from that of the simple SVD reconstruction. It is possible that a more sophisticated image-filtering algorithm, fusing the strong points of these two methods, could improve performance over either of them.

4. PROFILE ASSOCIATION

Computing the features is only half the job. Once we have feature measurements from a set of vehicles, we need an algorithm for deciding which vehicles are of the same class. One approach to the association problem is to compute a correlation coefficient; this is the approach used, e.g., in the SHARP algorithm.[3,4] A second approach, and the method described here, is to use one set of profiles, the *template* or *training* set, to build a statistical model for the feature, and compute the likelihoods of the features in the second set, the *test* set, given this model.

The model we have investigated most thoroughly is based on the beta distribution

$$P_B(x;\alpha,\beta) = \begin{cases} \dfrac{x^{\alpha-1}(1-x)^{\beta-1}}{\mathrm{B}(\alpha,\beta)} \equiv \dfrac{\Gamma(\alpha+\beta)}{\Gamma(\alpha)\Gamma(\beta)} x^{\alpha-1}(1-x)^{\beta-1} & \text{for } x \in (0,1) \\ 0 & \text{otherwise} \end{cases} \tag{5}$$

[‡]The SVD, as specified here, is not quite unique. For each set of k identical singular values $s_{i+1}, \ldots, s_{i+k}$ the product $USV^\dagger$ is preserved by a simultaneous $\mathsf{U}(k)$ rotation of $[\mathbf{u}_{i+1}, \ldots, \mathbf{u}_{i+k}]$ and $[\mathbf{v}_{i+1}, \ldots, \mathbf{v}_{i+k}]$. In addition, for any zero singular values there is an additional $\mathsf{U}(k)$ freedom since the rotations of the U and V subspaces no longer need be coupled. This nonuniqueness will not concern us here.

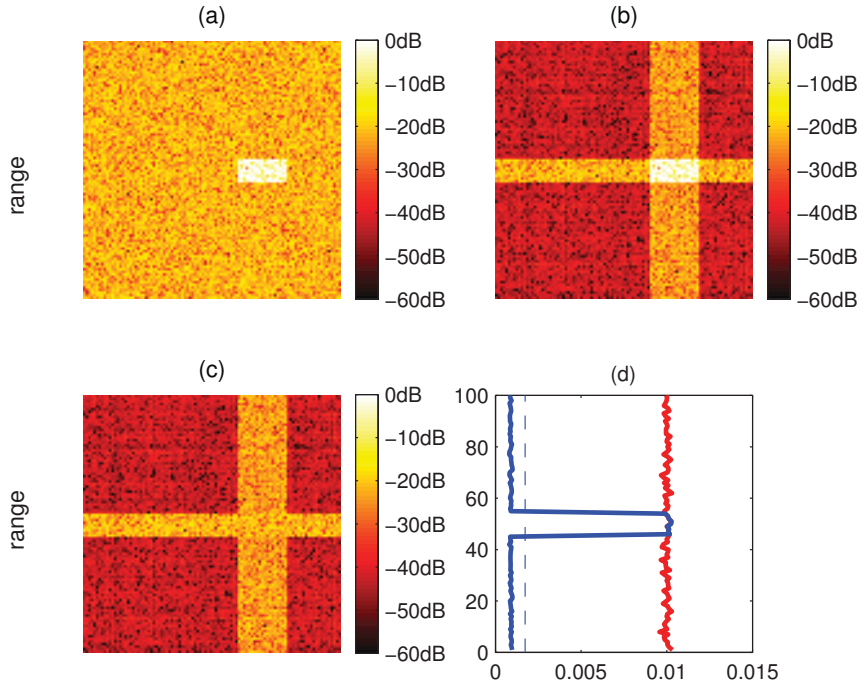

Figure 1. Notional example of SVD filtering, for a rectangular target 10 pixels by 20 pixels in size in a 100×100 image. The target-to-clutter ratio is about 40 dB (chosen to make the effect obvious in the images; the technique works for much lower target-to-clutter ratios as well). The image is reconstructed using a rank-10 SVD reconstruction. (a) The original image. (b) The rank-10 SVD-reconstructed image. (c) The SVD-reconstructed image with the original (clutter-free) target subtracted. The clutter level in target rows and columns is reduced only slightly, while the clutter level elsewhere in the image is reduced by about a factor of 10. (d) The clutter density integrated over the cross-range coordinate, for the original image (red) and the reconstruction (blue). The dashed blue line is the mean clutter value (over the profile) after reconstruction. Notice that the integrated clutter density at the target range remains essentially unchanged.

with two parameters $\alpha, \beta > 1$ and having mean and variance

$$\mu(\alpha,\beta) = \frac{\alpha}{\alpha+\beta} \quad , \quad \sigma^2(\alpha,\beta) = \frac{\alpha\beta}{(\alpha+\beta)^2(\alpha+\beta+1)} \quad . \tag{6}$$

We model the profile as a product of independent beta distributions, one for each range bin. From the template data set we fit the parameters α_r, β_r for each range bin (either by inverting the equations for $\mu(\alpha,\beta)$ and $\sigma^2(\alpha,\beta)$, or by computing the maximum-likelihood estimator); then we compute the likelihood of each test profile given this statistical model. That is, from each set of template data (derived from a single target over a small range of aspect angles) we derive a statistical model for the HRR profiles in that set,

$$\mathcal{M}(\mathbf{y}|\boldsymbol{\alpha},\boldsymbol{\beta}) = \prod_r P_B(y_r;\alpha_r,\beta_r) \; ; \tag{7}$$

then for each profile $\mathbf{y}$ to be tested we compute the likelihoods $\Lambda(\mathbf{y}|t) \equiv \mathcal{M}(\mathbf{y}|\boldsymbol{\alpha}_t,\boldsymbol{\beta}_t)$ for all templates t.

Note that this distribution is sensitive to range alignment between the profiles in the two sets. Because of the assumption that all range bins have independent distributions, this model cannot account for relative shifts between the template and test data. Poor alignment of *all* the data will effectively act to smear the profile in range, as if the range resolution is lower. But with poor alignment between the template and test profiles, the correct model will not, in general, form a good match to the profile. The requirement of range alignment means that data derived from images with different range pixel spacings must be resampled to a common sampling

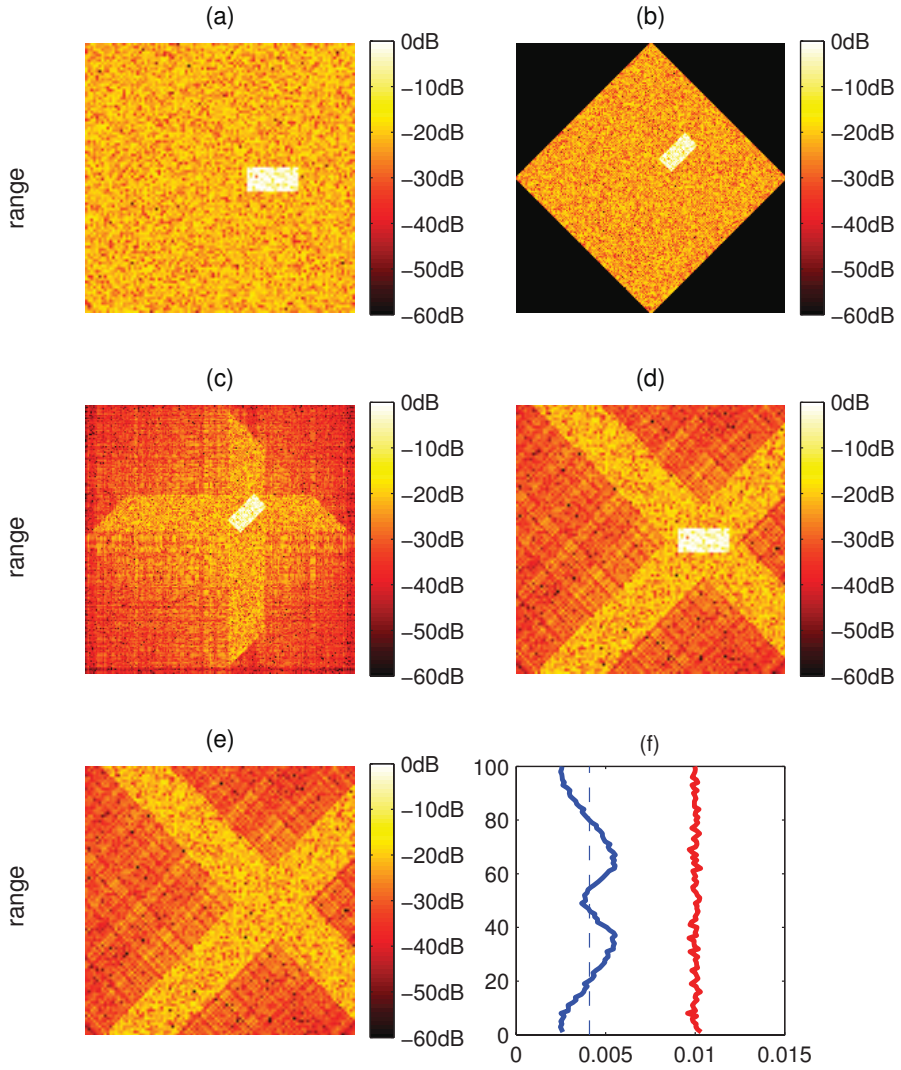

Figure 2. Notional example of rotated-SVD filtering, for the same situation as in Figure 1. The checkerboard matrix is larger, so a higher-rank reconstruction was used. This example shows a rank-27 reconstruction. (a) The original image. (b) The rotated image on the checkerboard lattice. (c) SVD reconstruction of the image of (b). (d) The image of (c), rotated back from the checkerboard lattice. This is the rotated-SVD reconstruction. (e) The reconstructed image with the original target subtracted. In this case the clutter level at the target rows and columns is noticeably reduced. (f) The clutter density integrated over the cross-range coordinate, for the original image (red) and the reconstruction (blue). The dashed blue line is the mean clutter value after reconstruction. Although the mean is larger than for the SVD method, the integrated clutter density at target ranges has dropped by a factor of about 2.

interval, and aligned with the same technique, for comparison. More general statistical models could be designed to account for such correlated differences between profiles.

Since these features are so strongly aspect dependent, the number of models created may be quite large; searching through such a database may be a daunting task. However, a newly-measured feature need not always be compared against all models in the database. From some combination of kinematic information in the same measurement and recent track information for its track, it is often possible to make a reasonable estimate of the vehicle's state, including its aspect, and only the models at the possible target aspects need be subjected to the full calculations of (7). (For ground vehicles traveling along roads, for example, the vehicle may be assumed to be oriented nearly parallel to the road direction. In other cases, the estimated velocity of a vehicle often provides

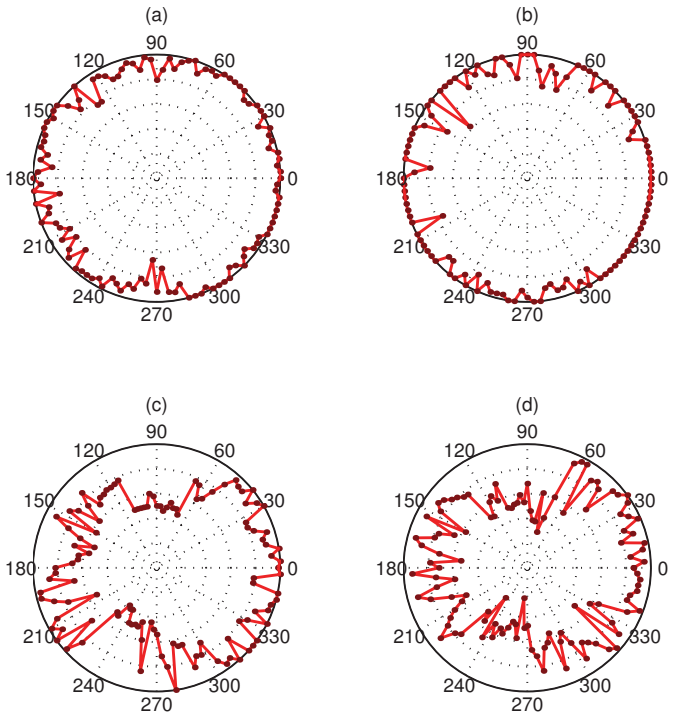

Figure 3. $P_{\rm cc}$ versus azimuth; no SVD filtering. (a) Train with MTI data; test with MTI data. (b) Train with SAR data; test with SAR data. (c) Train with MTI data; test with SAR data. (d) Train with SAR data; test with MTI data.

a good indicator of its aspect.) Given a probabilistic prior estimate $p(\Phi)$ of the aspect Φ for a feature y, the likelihood that this feature belongs to the class t of vehicle models must be computed as an average over the possible aspects:

$$\Lambda(\mathbf{y}|t) = \int_{\Phi} p(\Phi)\mathcal{M}(\mathbf{y}|\boldsymbol{\alpha}_{t,\Phi}, \boldsymbol{\beta}_{t,\Phi})\, d\Phi \ . \tag{8}$$

The likelihoods calculated by this association procedure can be used in any of several ways: A maximum-likelihood association (forced decision) can be made; there can be a likelihood threshold, below which decisions are postponed until new and hopefully better information arrives; or the likelihood vector may be used in a Bayesian evidence-update scheme to improve the classification of the target over time.

5. RESULTS

In Figures 3 and 4 we present some performance results and comparisons between the algorithms described above. In each figure are shown four polar plots of the probability of correct classification $P_{\rm cc}$ versus target azimuth, both with (Figure 4) and without (Figure 3) the application of SVD rank-reduction. The four graphs show results for all four comparisons of moving-target and stationary-target data, with training and testing data sets chosen from moving-target (MTI) and stationary-target (SAR) data, to simulate one of the difficult association problems described above.

The SVD-filtered results show noticeable improvement in the cross-association cases (training on the moving-target data and testing on the stationary-target data, or vice versa), at the cost of a slight reduction in $P_{\rm cc}$ for the cases in which training and testing are performed on the same type of data. Not shown are results using the rotated-SVD rank-reduction technique, which provides performance similar to that of the SVD method; and results using the dominant-scatterer method $y_r^{(\infty,1)}$, which provides performance similar to the original $y_r^{(1,1)}$ profiling algorithm.

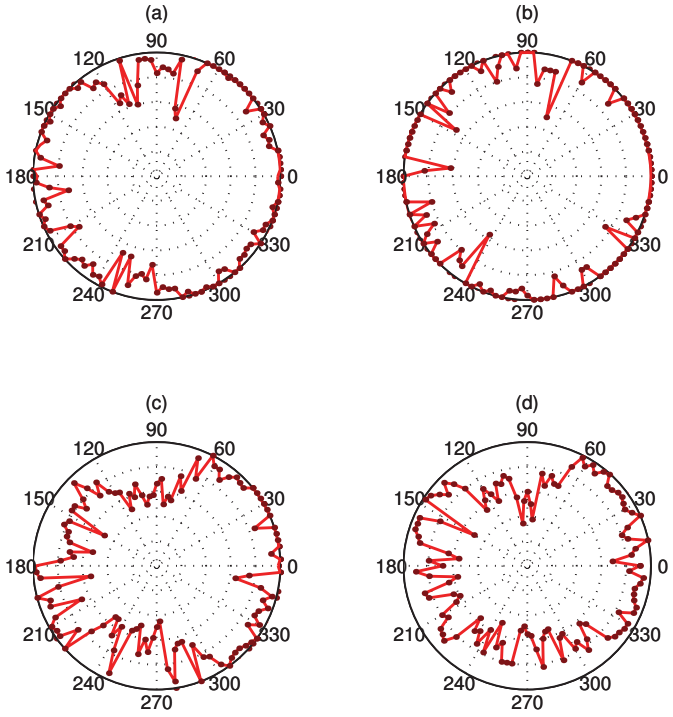

Figure 4. P_{cc} versus azimuth; SVD filtering performed before cross-range integration. (a) Train with MTI data; test with MTI data. (b) Train with SAR data; test with SAR data. (c) Train with MTI data; test with SAR data. (d) Train with SAR data; test with MTI data.

6. CONCLUSION

We have described an algorithm for automated target recognition which allows both class-independent and class-dependent associaton. This algorithm allows comparison between radar measurements of different types (e.g. MTI range-Doppler and SAR images) and is based on the extraction of one-dimensional range signatures, or high-resolution range profiles, from the images, and the construction of statistical models based on these signatures. Techniques for reducing the clutter density in the images show potential to improve performance, especially in comparisons involving different measurement types.

REFERENCES

1. B. Hodges, 2002. Private communication.
2. C. Oliver and S. Quegan, *Understanding Synthetic Aperture Radar Images*, Artech House, Boston, 1998.
3. J. Westerkamp, "A framework for 1-D HRR ATR evaluation," tech. rep., AFRL/SNAT, 1998.
4. M. B. Ressler *et al.*, "Robust automatic target recognition (ATR) using HRR profiles," tech. rep., Toyon Research Corporation, 2000.